Prepared for submission to JCAP

arXiv:1808.00464v1 [astro-ph.GA] 1 Aug 2018

First constraints on Fuzzy Dark Matter from the dynamics of stellar streams in the Milky Way

Nicola C. Amorisco[a,b] **, A. Loeb**[a]

[a]Institute for Theory and Computation, Harvard-Smithsonian Center for Astrophysics, 60 Garden St., MS-51, Cambridge, MA 02138, USA

[b]Max Planck Institute for Astrophysics, Karl-Schwarzschild-Strasse 1, 85748 Garching, Germany

E-mail: nicola.amorisco@cfa.harvard.edu

Abstract. We present a novel method to constrain the mass of ultra-light bosons as the dark matter using stellar streams formed by disrupting Globular Clusters in the Milky Way. The turbulent density field of Fuzzy Dark Matter (FDM) haloes results in perturbations and dynamical heating of thin streams. Using numerical simulations based on an effective model, we explore the magnitude of this phenomenon and show that this is observable for the range of axion masses m_a that is interesting for alleviating the 'small-scale problems' of ΛCDM. We derive an analytical model for the thickening of thin stellar streams and obtain an early conservative lower limit for the boson mass of $m_a > 1.5 \times 10^{-22}$ eV, using pre-Gaia literature data for six Milky Way streams and after marginalizing over physical parameters. This demonstrates the great promise for using this novel dynamical method as a fully independent probe of FDM, to complement results based on Lyman-α forest data.

Contents

1 Introduction **1**

2 Dynamical heating of cold stellar streams **2**
2.1 An effective model: 'quasiparticles' 3
2.2 An analytical model of the stream thickness 3
2.2.1 Vertical angular width 3
2.2.2 Angular width in the orbital plane 5
2.2.3 Magnitude of the heating effect 7

3 Numerical examples **7**
3.1 Effective FDM clumps in *Gadget 2* 7
3.2 The suite of runs 9
3.3 Tests of the analytic model 11

4 First constraints on the axion mass **13**

5 Discussion and Conclusions: an independent dynamical probe of FDM **15**

1 Introduction

Ultra-light bosons [1–3] have been proposed as a viable alternative to cold dark matter (CDM) [4–8]. A bosonic scalar field is compatible with current cosmological constraints [9–11], as it behaves like CDM on large scales. However, the two models differ at non-linear scales for axion masses $m_a \lesssim 10^{-21}$ eV, corresponding to a de Broglie wavelength of ~ 1 kpc. Differences include a suppression in the small-scale power spectrum [12–14] and the formation of centrally cored dark matter haloes [15, 16], both of which could ease some of the small-scale challenges of galaxy formation in CDM [17, 18]. For instance, an axion mass of $m_a \lesssim 2\times10^{-22}$ eV would reproduce the observed kinematics of multiple stellar sub-populations in the Milky Way dwarf Spheroidal satellites [19–21], without the need to invoke the strong stellar feedback required in CDM [22, 23]. As such, Fuzzy Dark Matter (FDM) has recently attracted attention as a viable alternative to CDM.

A number of analytic studies have addressed the properties of dark matter haloes in FDM, predicting the formation of a stable self-gravitating Bose-Einstein condensate characterized by a central constant-density core [24–26]. Recent numerical studies [27, 28] have confirmed this prediction and showed that, as in CDM, the density profile of FDM haloes is well fit by a Navarro-Frenk-White profile [NFW, 29], in which the most central region of the cusp is replaced by the soliton core. The size of the latter varies with both halo mass M_{vir} and m_a [27, 28]: for a Milky Way sized halo with $M_{vir} = 10^{12} M_\odot$, it is $r_{sc} \sim 0.2/m_{22}$ kpc, where $m_a = m_{22} \times 10^{-22}$ eV.

Both analytic work and numerical simulations have shown that FDM haloes are characterized by a sustained turbulent behavior, with order unity oscillations in the density field [27, 28, 30]. These fluctuations, in the form of soliton-sized clumps [27], are caused by the reconnection of quantum vortex lines [28], a phenomenon that is shared by Bose-Einstein condensates in absence of self-gravity [31, 32]. Turbulence may cause observable dynamical

heating, offering means to constrain m_a. However, Ref. [18] finds that the timescales for *(i)* the disruption of binary stars, *(ii)* the thickening of the Galactic disk and *(iii)* the heating of open and globular clusters (GCs), are exceedingly long for these processes to provide useful constraints[1]. Here, we explore the dynamical heating of stellar streams of disrupting GCs, using both analytic and numerical methods. We set out to investigate what is the magnitude of the effect of quantum turbulence on the dynamics of GC streams in the interesting range of axion masses. We find that thin, kinematically cold stellar streams in the Milky Way represent a promising dynamical probe of the axion mass, providing means to set local dynamical constraints to this alternative dark matter model.

In Section 2 we derive an analytical model for the dynamical heating of stellar streams, which we test using effective numerical simulations in Section 3. In Section 4 we use pre-Gaia literature data for a selection of Milky Way GC to illustrate the promise of this novel method and to derive a first constraint on the axion mass.

2 Dynamical heating of cold stellar streams

Due to their internal dynamical coherence (internal velocity dispersion $\lesssim 1$ km s^{-1} [33, 34]) GC streams are excellent gravitational detectors of dark matter subhaloes [35–40] and other baryonic disturbances [41–43]. In FDM, GC streams experience the additional perturbing effects of quantum fluctuations.

There are two qualitative differences between the disturbances due to the flyby of dark matter subhaloes in a ΛCDM halo and those due to FDM granules.

- First, the mass fraction in bound subhaloes in the central regions of a Milky Way sized halo is of only a few per cent [44–47], implying a limited number of encounters per stream [48]. It follows that the strongest observable perturbations – in the form of density 'gaps' and associated kinematic disturbances – are due to the rare encounters with the most massive subhaloes, a process that is stochastic in nature. Instead, when orbiting a FDM halo, streams experience the continuous, recurring perturbations of quantum turbulence. For axion masses $m_{22} \gtrsim 1$, each single encounter with a soliton-sized quantum density fluctuation has a limited perturbing effect. However, since all of the dark matter participates in the turbulence (rather than just a small fraction), the rate of flybys is high. This results in an inevitable process of diffusive heating.

- The second qualitative difference has to do with the opposite dependences of the strength of the perturbing effects with galactocentric radius.While ΛCDM subhaloes become rarer in the innermost regions of the halo [44–46] making stochasticity ever more important, in FDM perturbations increase with decreasing radius, as the order-unity density fluctuations scale with the local dark matter density itself [18].

Simulating a Milky-Way sized FDM halo self-consistently and resolving the dynamics of individual quantum clumps is extremely challenging at the moment, especially for the range of axion masses that is most interesting, $m_{22} \gtrsim 0.1$. Even more difficult would be to also resolve the internal dynamics of a GC and its stream in such a self-consistent FDM simulation. Therefore, here we provide a first quantification of the effect of quantum turbulence based on an effective description of the turbulent density field of FDM haloes.

[1] Except possibly for the case of GCs close to the Galactic center.

2.1 An effective model: 'quasiparticles'

In order to quantify the dynamical heating of a thin stellar stream, we follow Ref. [18] and adopt a phenomenological model of the density fluctuations in FDM haloes, describing quantum clumps with 'quasiparticles'. We base this model on the results of recent self-consistent simulations [27, 28]: quasiparticles have a mass

$$M_{eff} = \rho V_{cl} = 4\pi\rho r_{sc}^3/3 \ , \tag{2.1}$$

with ρ being the time-averaged local dark matter density and r_{sc} being the size of the halo's soliton core, $r_{sc} = r_{sc,1}/m_{22}$ kpc. Using the soliton radius appropriate for a Milky Way sized halo, $r_{sc,1} = 0.2$ kpc, Eqn. (2.1) implies that the mass of quantum clumps at the solar radius ($\rho_\odot = 10^7 M_\odot$ kpc^{-3}, [49]) is

$$M_{eff,\odot} = 3.4 \times 10^5 \ m_{22}^{-3} \ M_\odot \ , \tag{2.2}$$

showing the steep dependence on the axion mass. We assume that effective FDM clumps have a smooth density profile, represented by Plummer spheres with a smoothing length $\epsilon = r_{sc}$, and that they move within the halo potential with velocities appropriate for an isotropic system in dynamical equilibrium.

The choices above should be intended as temporary working assumptions, broadly guided by the results of currently available self-consistent FDM simulations. For instance, we are using that all quantum clumps at some given radius have the same effective mass M_{eff}, while it is likely that a distribution of masses would be more appropriate. In turn, such a distribution might also include secondary dependences on galactocentric radius, or on clump velocity. Future self-consistent simulations will provide a better characterisation of the sustained turbulent density field of FDM halos, allowing for a more faithful description of the spectrum of effective masses, clump velocities, smoothing radii, as well as of any correlations between these properties. It is straightforward to take these into account within the framework of the analytic model we are about to set out.

2.2 An analytical model of the stream thickness

We consider a stellar stream with orbit $r(t)$ and we wish to describe the thickening caused by the continuous encounters with the FDM clumps. We consider the conservative case of a spherically symmetric underlying gravitational potential, since this minimizes the growth rate of the stream thickness [50, 51]. The dynamics of tidal streams within their orbital plane and perpendicularly to it are qualitatively different, therefore we treat these two degrees of freedom separately. We use the symbol $\omega_\parallel$ to indicate the angular width of the stream in the orbital plane and ω_z for the angular width perpendicularly to the orbital plane. The observed angular width of any given stream on the sky can be obtained as a combination of the two, which of course depends on the viewing angle.

2.2.1 Vertical angular width

The thickness of a tidal stream in the direction perpendicular to the orbital plane, $\hat{\mathbf{z}}$, is due to the misalignment of the orbital planes of its member stars [51–53]. Encounters with the quantum granules cause additional scattering of such individual planes. Following an encounter and a velocity change $\delta\mathbf{v}$, a star's orbital plane is tilted by the angle

$$\delta\theta = \arctan\left(\delta v_z / v_\phi\right) \approx \delta v_z / v_\phi \ , \tag{2.3}$$

where v_ϕ is the angular velocity of the stream at the location of the encounter. We assume that the process is a diffusive one, i.e. that the number of encounters is large enough that the mean orbital plane of the stream is unchanged and that individual encounters are uncorrelated. In this case FDM turbulence causes a vertical thickening rate of

$$\frac{d\langle\omega_z^2\rangle}{dt} \approx \left\langle \iint f(r, \mathbf{v_{cl}}) d^3\mathbf{v_{cl}}\ 2\pi b db\ n\ v_{rel} \left(\frac{\delta v_z}{v_\phi}\right)^2 \right\rangle_{r(t)} , \tag{2.4}$$

where $f(r, \mathbf{v_{cl}})$ is the distribution of clump velocities at radius r, b is the impact parameter, $n = 1/V_{cl}$ is the number density of clumps, v_{rel} is the relative velocity between star and clump. All of v_{rel}, δv_z and v_ϕ depend on the proper velocity of the clump $\mathbf{v_{cl}}$ and on the specific orbit of the stream, $r(t)$, at the location of the encounter. We use the symbol $\langle\cdot\rangle_{r(t)}$ to indicate the average over one radial orbital period. Making use of the impulse approximation and absorbing all dependences on the stream orbit in the average g_z, we obtain

$$\frac{d\langle\omega_z^2\rangle}{dt} \approx \frac{16\pi^{3/2}}{\sqrt{3}} \ln\Lambda \frac{G^2\rho^2(r_c)}{v_c^3(r_c)} g_z^2\left[r(t)\right]\ r_{sc,1}^3\ m_{22}^{-3} , \tag{2.5}$$

where $\ln\Lambda$ is the classical Coulomb logarithm, which we estimate in Sect. 3 using a suite of numerical experiments. As expected for a diffusive process, the vertical angular thickness grows approximately like $\langle\omega_z^2\rangle \propto t$.

Given the stream orbit $r(t)$, a model for the gravitational potential of the Milky Way and a probabilistic description of the properties of FDM clumps, the dimensionless quantity g_z can be calculated exactly. We use the working assumptions listed in Sect. 2.1 and consider the case in which the underlying gravitational potential and time-averaged dark matter density distribution are approximately scale-free. In this case g_z does not depend on the orbital energy of the stream, but only on its circularity j. Here $j \equiv J/J_c(E)$, where J is the angular momentum and $J_c(E)$ is the angular momentum of a circular orbit with the same energy E, corresponding to the radius r_c and to a circular velocity $v_c(r_c)$.

The full red line in Figure 1 shows the magnitude of the function $g_z(j)$ for the case of an underlying logarithmic gravitational potential, $\Phi(r) = v_c^2 \log(r)$, corresponding to a total density distribution $\rho \propto r^{-\gamma}$, with $\gamma = 2$. This explicitly uses the properties of orbits in such a potential, while assuming that the distribution of clump velocities $f(r, \mathbf{v_{lc}})$ is Maxwellian and isotropic, with constant 1-dimensional velocity dispersion $\sigma_{cl} = v_c/\sqrt{2}$. The resulting g_z is a monotonic function of j, and increases for streams on eccentric orbits. This should be expected as, all the rest being the same, encounters close to orbital apocenter are more effective at tilting a star's orbital plane, as can be gathered by Eqn. (2.3). We also consider the case $\gamma = 1$, describing the inner regions of an NFW density profile, and show the corresponding function g_z with a red dashed line in the same Figure. It appears that the average g_z is only marginally sensitive to the detailed properties of the underlying potential.

The thickening captured by Eq. (2.5) is cumulative: regions of the stream that are further away from the progenitor have been shedded at an earlier time and are therefore predicted to have grown hotter and thicker after interacting with the quantum clumps for longer periods of time. If we consider the stars at a distance l along the stream from the progenitor GC and assume these have been orbiting freely for a time $t = t(l)$ after being tidally stripped, the vertical angular thickness at that location in the stream is:

$$\langle\omega_z^2\rangle^{1/2}(l) = \left(\omega_{z,0}^2 + \frac{d\langle\omega^2\rangle}{dt} t\right)^{\frac{1}{2}} . \tag{2.6}$$

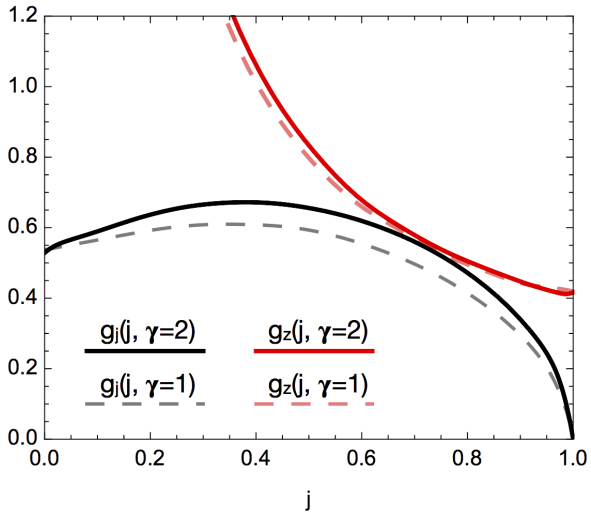

Figure 1. : The functions $g_z(j)$ and $g_j(j)$ describing the diffusive thickening of streams in FDM haloes, as in Eqs. (2.5) and (2.11). Full lines refer to the case of streams orbiting an underlying logarithmic spherically symmetric gravitational potential, corresponding to a power law exponent $\gamma = 2$ for the total density profile. Dashed lines refer to the central regions of a total density profile with power law index $\gamma = 1$, as in the case of an NFW halo.

Here, $\omega_{z,0}$ is the vertical angular width of an unperturbed stream, which is constant in time if the background potential is spherically symmetric.

Since the growth in the length of the stream is secular, $l(t) \propto t$, the effect of FDM turbulence should manifest itself in streams with flaring vertical density profiles, i.e. with a vertical thickness that increases while moving away from the remnant of the progenitor, with a behavior $\omega_z(l) \propto l^{1/2}$. In practice, a prediction for the local angular width as function of position along the stream is especially challenging, first of all because the location of the remnant itself is unknown for most Milky Way GC streams. Additionally, a detailed estimate of the stream age as a function of location requires a precise knowledge of GC mass and internal kinematics, stream orbit and Milky Way potential, all of which influence the speed at which the stream grows in length [48, 52, 53]. For these reasons, we also estimate a mean global angular thickness for the entire stream, $\langle\omega_z^2\rangle^{\frac{1}{2}}$, averaged over its full length:

$$\langle\omega_z^2\rangle^{\frac{1}{2}}(t) = \left(\omega_{z,0}^2 + \Gamma_z \frac{d\langle\omega^2\rangle}{dt} t\right)^{\frac{1}{2}} \quad , \tag{2.7}$$

The magnitude of the coefficient Γ_z depends on the time dependence of the mass loss rate of the parent GC. Assuming this is approximately constant in time [54, 55] gives us

$$\Gamma_z \equiv \int_0^1 \lambda^2 d\lambda = \frac{1}{3} \, . \tag{2.8}$$

2.2.2 Angular width in the orbital plane

In the plane of the orbit, the angular width of a stream is due to the spread in the angular momentum of its stars [52, 53]. Stars move away from the progenitor GC at a speed that depends on their energy, so that stars at a specific location along the stream have similar orbital energies [52, 53]. The angular width of the stream in the orbital plane therefore

reflects the spread in orbital circularities: the angle between two different stars with similar energy but differing by δj is

$$\delta\phi \approx \frac{\partial\phi}{\partial j}\,\delta j\,\frac{t}{T_r}\,, \tag{2.9}$$

where T_r is the radial period of the stream and ϕ is the corresponding azimuthal angle. Note that such angular distance grows secularly, implying that even when unperturbed the stream phase mixes with time within the orbital plane.

To add to this, scattering with the quantum clumps causes the spread in circularities of stars in the stream to progressively grow with time. Assuming again the number of encounters is sufficiently large, the relevant diffusion is

$$\frac{d\langle\delta j^2\rangle}{dt} \approx \left\langle \iint f(r,\mathbf{v_{cl}})d^3\mathbf{v_{cl}}\;2\pi b db\;n\;v_{rel}\;\delta j^2(\delta\mathbf{v})\right\rangle_{r(t)} \tag{2.10}$$

where $\delta j(\delta\mathbf{v})$ is the change in circularity caused from the velocity change $\delta\mathbf{v}$. The change $\delta j(\delta\mathbf{v})$ depends on the clump velocity $\mathbf{v_{cl}}$ and on the specific location of the encounter, through the orbit of the stream $r(t)$. As for Eqn. (2.5), we use the impulse approximation and absorb all dependences on the stream orbit in an average g_j, to get

$$\frac{d\langle\delta j^2\rangle}{dt} \approx \frac{16\pi^{3/2}}{\sqrt{3}}\ln\Lambda\frac{G^2\rho^2(r_c)}{v_c^3(r_c)}g_j^2\left[r(t)\right]\;r_{sc,1}^3\;m_{22}^{-3}\,. \tag{2.11}$$

Figure 1 shows the magnitude of the function $g_j(j)$ for the cases of an underlying logarithmic gravitational potential and for the case of a cuspy NFW total density profile.

As for the stream's effective vertical velocity dispersion, the stream's spread in circularity also grows as expected for a diffusive process: $\langle\delta j^2\rangle \propto t$. However, the coupling with the intrinsically secular dynamics of the stream captured by Eqn. (2.9) causes the stream thickness in the orbital plane to grow in a quicker fashion[2]. At a location l along the stream, composed of stars that have been tidally lost at a similar time $t(l)$ in the past, the local angular thickness in the orbital plane is

$$\langle\omega_\parallel^2\rangle^{1/2}(l) \approx \left[\omega_{\parallel,0}^2(t) + \Gamma_l\left(\frac{\partial\phi}{\partial j}\right)^2\frac{d\langle\delta j^2\rangle}{dt}\frac{t^3}{T_r^2}\right]^{\frac{1}{2}}\,, \tag{2.12}$$

The coefficient Γ_l accounts for the formal convolution of both thickening effects: the spread in circularity grows diffusively thanks to the FDM clumps, and this growth is then secularly amplified by the stream's own internal dynamics:

$$\Gamma_l \equiv \int_0^1 (1-\lambda)\lambda^2 d\lambda = \frac{1}{12}\,. \tag{2.13}$$

When orbiting in a smooth potential the angular thickness in the orbital plane should flare like $\omega_{\parallel,0}(l) \propto l$, due to inevitable phase mixing. The quicker flaring, $\omega_\parallel(l) \propto l^{3/2}$, testifies the presence of a turbulent density field. Averaging over the full stream of age t, we get a global mean angular width of

$$\langle\omega_\parallel^2\rangle^{\frac{1}{2}}(t) = \left[\omega_{\parallel,0}^2(t) + \frac{\Gamma_\parallel}{12}\left(\frac{\partial\phi}{\partial j}\right)^2\frac{d\langle\delta j^2\rangle}{dt}\frac{t^3}{T_r^2}\right]^{\frac{1}{2}}\,, \tag{2.14}$$

[2]Deviations from spherical symmetry in the background potential introduce an analogous coupling in the evolution of the vertical thickness, but we do not consider this effect here.

where, due to the different dependence with time/location, $\Gamma_\parallel \neq \Gamma_z$, and, for a constant mass loss rate, $\Gamma_\parallel = 1/4$.

In the following, we make the conservative choice of taking a constant $\omega_{\parallel,0}$, as, in practice, its growth rate depends critically on the poorly known mass of the progenitor GC and on the detailed properties of the Milky Way potential [53]. We calibrate both vertical and parallel unperturbed widths using a suite of numerical simulations of perturbed and unperturbed streams in Sect. 3, where we also show that a Coulomb logarithm of magnitude $\ln\Lambda \approx 9.6$, constant in time, well describes the evolution of streams following a variety of orbits in our numerical experiments.

2.2.3 Magnitude of the heating effect

We use the model just described to illustrate with an order of magnitude estimate the importance of dynamical heating for GC streams in the Milky Way. For a dark matter density of $\rho_\odot = 10^7 M_\odot$ kpc^{-3} at the solar radius $R_\odot$, a circular velocity of $v_c = 220$ km s^{-1} and the most conservative case of a stream on a circular orbit, $j = 1$, Eqn. (2.5) predicts a vertical thickening rate of

$$\left.\frac{d\langle\omega_z^2\rangle}{dt}\right|_\odot \approx \left(0.2 \text{ deg} \times \frac{R_\odot}{r_c} \times m_{22}^{-1.5}\right)^2 \Big/ \text{Gyr} \,, \tag{2.15}$$

corresponding to an increase in the effective vertical velocity dispersion of the stream of

$$\left. v_c^2 \frac{d\langle\omega_z^2\rangle}{dt}\right|_\odot \approx \left(0.8 \text{ km s}^{-1} \times \frac{R_\odot}{r_c} \times m_{22}^{-1.5}\right)^2 \Big/ \text{Gyr} \,, \tag{2.16}$$

These figures are comparable in magnitude with the observed properties of thin GC streams in the Milky Way [33, 34, 56–58], showing that cold stellar stream can indeed provide a useful probe in the interesting range of axion masses. In fact, depending on the viewing angle of the stream, the observed thickening may be substantially larger, due to the different scaling of Eqns. (2.7) and (2.14). As mentioned in Sect. 2, heating is also predicted to become stronger towards the central regions of the Galaxy, where the local dark matter density increases, implying a corresponding increase in the mass of the quantum clumps, Eqn. (2.1). Assuming the density profile of the Milky Way is well described by an NFW profile results in the inverse scaling with radius of Eqns. (2.15) and (2.16). We come back to this in Sect. 5.

3 Numerical examples

We use a suite of N-body simulations to exemplify the heating of thin streams in FDM haloes and to test the analytic description developed in Sect. 2. Our simulations are based on the publicly available N-body code *Gadget 2* [59], which we however modify to introduce the phenomenological quasiparticle model described in Sect. 2.1.

3.1 Effective FDM clumps in *Gadget 2*

In each of our effective N-body simulations, we follow the evolution of a GC and its stream for 10 Gyr. We inizialize the GC so that its orbital plane is $z = 0$, and its angular momentum is $\mathbf{J_{GC}} = J_{GC}\hat{\mathbf{z}}$. Since we do not wish to use these simulations to directly reproduce the properties of observed streams, we can adopt a simplified mass model for the Galaxy. We assume that the total background potential follows a spherically symmetric NFW density distribution, with dimensional scalings appropriate for a Milky Way sized dark matter halo

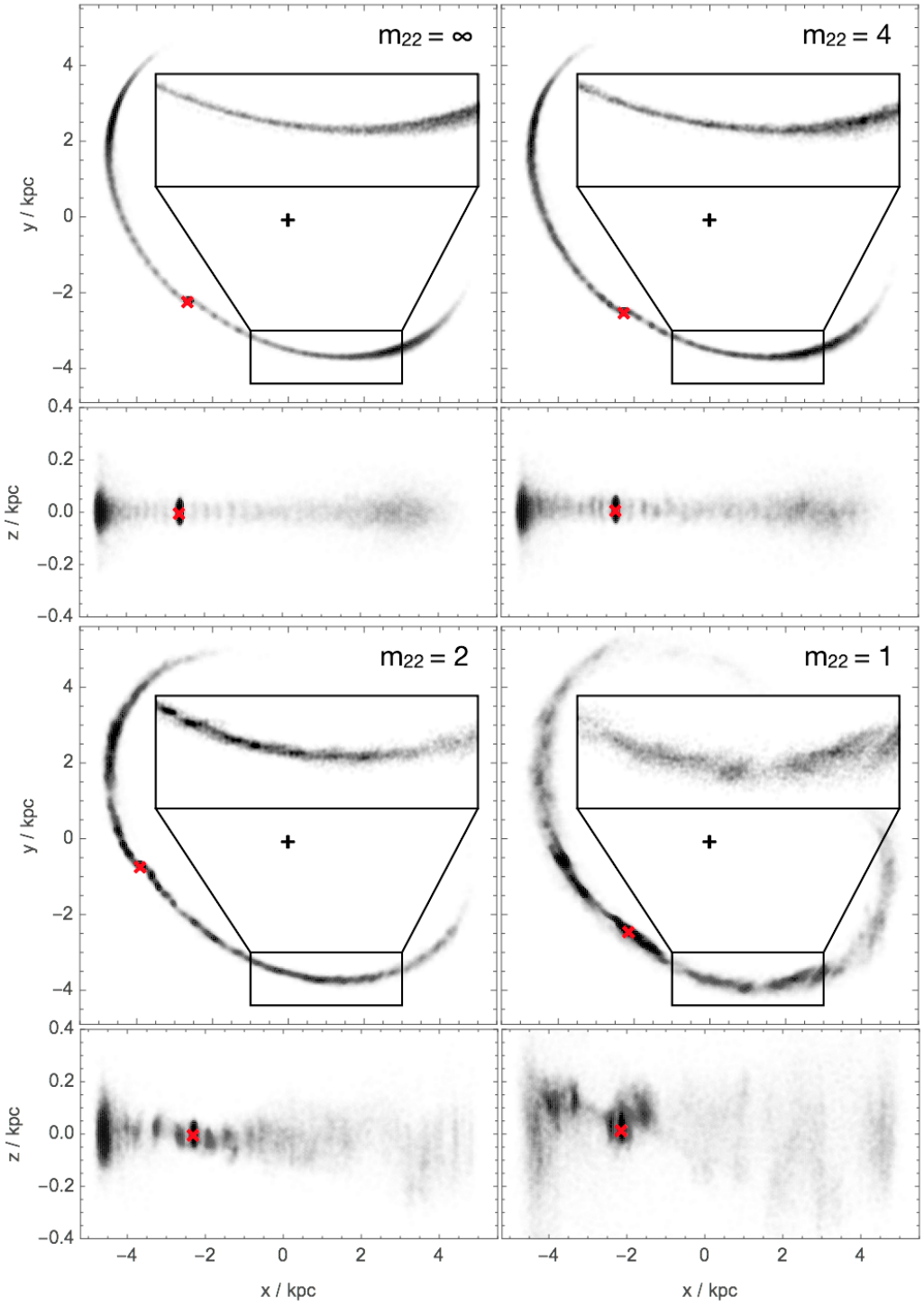

Figure 2. The density distributions of identical GC streams ($r_c = 4.4$ kpc, $j = 0.9$) evolved for 3 Gyr in Milky Way sized FDM haloes with decreasing axion mass. Upper panels show projections in the plane of the orbit, lower panels show vertical projections.The red cross indicates the position of the remnant.

(characteristic radius $r_0 = 20.6$ kpc, characteristic density $\rho_0 = 6.1 \times 10^6 M_\odot$ kpc^{-3}). This is the same as the time-averaged density distribution associated to the quantum clumps themselves.

In order to keep the number of 'live' quasiparticles and the computational effort reasonable, we represent the gravitational field of the FDM halo using the combination of a static, smooth background gravitational potential and live quantum clumps. The static gravitational potential is the one appropriate for the mass model of the Galaxy above. Then, we add a population of live quasiparticles, but only do so in the vicinity of the GC stream. In practice, at any single time, our simulations include live quasiparticles in the region $|z| < z_{max}$ (and $r < r_{max}$), where we take care to fix z_{max} (as well as r_{max}) such that this remains several times wider than the stream itself, during its entire evolution. This keeps the number of quasiparticles manageable and allows us to neglect the 'additional' mass introduced by the live clumps, which is always negligible with respect to the one imposed by the static potential, which drives the undisturbed dynamics of the stream.

According to the prescription of Eqn. (2.1), clumps have a uniform number density, $n = 1/V_{cl}$, which we use to generate the initial conditions of our live quasiparticles, randomly filling the volume within the boundary $|z| < z_{max}$. Eqn. (2.1) also prescribes that the mass of individual quasiparticles varies with radial location. For simplicity, we force our effective clumps to move on circular orbits, which keeps their individual mass constant in time. When the dynamics of individual quantum clumps is better resolved in self-consistent FDM simulations, this may be changed. For now, we assume quantum clumps move on randomly oriented orbital planes, with constant circular velocities, sampled from a Maxwellian distribution with dispersion that depends on radius, tracking the velocity dispersion of an isotropic dark matter halo with the same density profile. When individual quasiparticles cross the boundary $|z| = z_{max}$ and move out of the turbulent region, we individually replace them. We do so by introducing a new live clump which enters the turbulent region: we sample a new orbital radius together with new direction and magnitude for its angular momentum. This ensures that number density of live quasiparticles remains constant as well as approximately uniform during the entire simulation.

Within this strategy it is easy to track the location of each live quasiparticle in the simulation, analytically. We modify *Gadget 2* to do so and to calculate the perturbing force that each clump exerts on the stars that compose the GC and stream. We recall that we assume that effective clumps are represented by Plummer spheres, with a half-mass radius $\epsilon = r_{sc}$.

3.2 The suite of runs

In each run, the progenitor GC is represented by a live isotropic Plummer sphere, sampled with 10^5 equal mass particles. We explore a sample of different properties for the progenitor GC: we consider progenitors with masses in the range $4 \leq \log M_{GC}/M_\odot \leq 4.8$, and initial half-mass radii in the range $6 \leq r_{eff}/\mathrm{pc} \leq 16$. We also explore different orbits. We consider the case of an almost circular orbit, circularity $j = 0.9$, and the case of a significantly eccentric orbit $j = 0.6$. For the former, we consider two different orbital energies, $r_c = 7.8$ kpc, corresponding to a stream that orbits close to the solar radius, and $r_c = 4.4$ kpc, corresponding to a stream that inhabits the central regions of the Galaxy. The orbital energy of the eccentric case is $r_c = 6.3$ kpc. For each of these three orbits we simulate multiple instances of the cases $m_{22} = 1$, $m_{22} = 2$, $m_{22} = 4$.

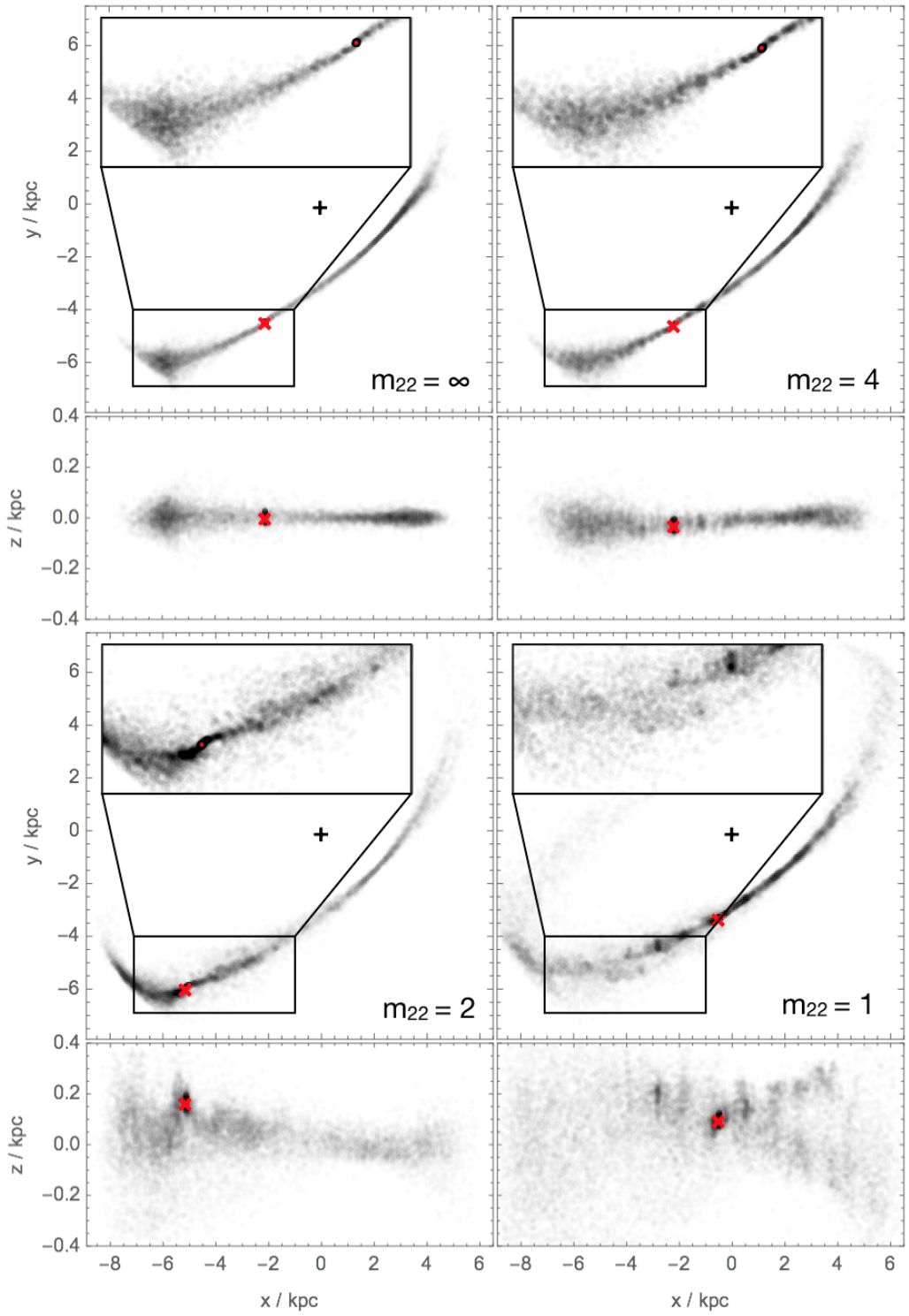

Figure 3. The density distributions of identical GC streams ($r_c = 6.3$ kpc, $j = 0.6$) evolved for 4.9 Gyr in Milky Way sized FDM haloes with decreasing axion mass. Upper panels show projections in the plane of the orbit, lower panels show vertical projections.The red cross indicates the position of the remnant.

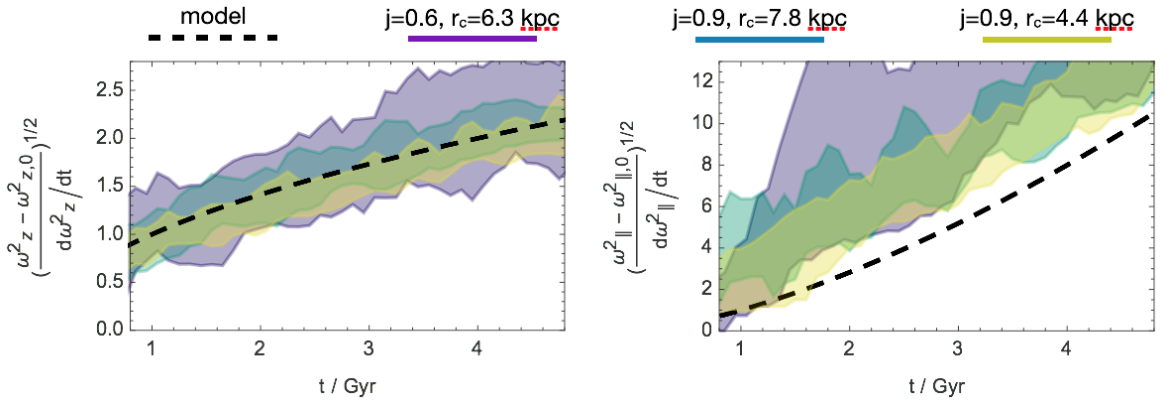

Figure 4. A comparison between our analytic model for the stream thickening (black dashed lines) and results from our suite of numerical experiments. Shaded areas (10-to-90% quantiles) pertain numerical results for sets of streams with the same orbital properties (as in the legend). Different axion masses and progenitor properties are explored for each orbit.

Figure 2 shows the density distributions of otherwise identical streams evolved in FDM haloes with different m_a, at $t = 3$ Gyr. The displayed snapshots refer to the case of GCs on the orbit $(j, r_c) = (0.9, 4.4$ kpc$)$, with identical progenitors with $\log M_{GC}/M_\odot = 4$ and $r_{eff} = 6$ pc. The case $m_{22} = \infty$ shows the case of an unperturbed stream, orbiting only under the influence of the smooth and static background potential, with no live clumps. For decreasing values of m_{22} streams become gradually kinematically hotter and thicker. Figure 3 shows similar snapshots for streams generated by progenitor GCs with the same properties, but on a different orbit, with energy $r_c = 6.3kpc$ and significantly more eccentric $j = 0.6$. The snapshots show the stream after $t = 4.9$ Gyr of evolution.

Figs. 2 and 3 also show that streams become increasingly disturbed and structured with decreasing axion mass. This applies to both their density distributions and kinematics. This behavior is due to the quickly increasing mass of individual quantum clumps, Eqn. (2.2), as well as to number of individual encounters experienced by the stream, which decreases at the same rate. When axion masses are $m_{22} \lesssim 1$ individual encounters may be effective enough to cause the formation of gaps and kinks in the stream, as for the case of dark matter subhaloes and giant molecular clouds. Differently from what happens for higher axion masses, these encounters shape the structure of the stream with individual features. These are more persistent when $m_{22} \lesssim 1$ as longer times are required for subsequent encounters to erase them, due to the reduced rate of flybys.

These 'large-scale' perturbations are not explicitly predicted by our diffusive model, which is based on the assumption of a large number of uncorrelated encounters. Rather than causing displacements in the mean location of the stream, uncorrelated encounters simply increase its width in phase space. However, as we show in the following Section, we still find that our analytic model provides a good description of the evolution of the average width of the stream, at least within the range of axion masses we explore, $m_{22} \geq 1$.

3.3 Tests of the analytic model

Figure 4 compares the global mean angular width of streams in our numerical suite with the predictions of our analytic model. The left panel pertains to the vertical angular width,

and displays results in terms of the quantity $\left(\frac{\omega_z^2-\omega_{z,0}^2}{d\omega_z^2/dt}\right)^{\frac{1}{2}}$. Streams with different progenitors and orbits have different constant undisturbed widths $\omega_{z,0}^2$. Different axion masses as well as stream orbits imply different growth rates $d\omega_z^2/dt$. However, according to Eqn. (2.7), our model predicts that this combination should scale simply as

$$\left(\frac{\omega_z^2-\omega_{z,0}^2}{d\omega_z^2/dt}\right)^{\frac{1}{2}} = t^{\frac{1}{2}} \ . \tag{3.1}$$

The black dashed curve in left panel of Fig. 5 displays such scaling. Shaded areas are simulation results. They group all streams in our suite with the same progenitor's orbit, and extend between the 10% and 90% quantiles over the different set of realizations. We measure the mean vertical angular width using all particles that are no longer bound to the progenitor GC, and calculating the standard deviation of the distribution of individual inclinations $\omega_z = \arctan\left(z/\sqrt{x^2+y^2}\right)$.

We use a simple model for the unperturbed vertical width

$$\omega_{z,0} = k_z \left[\frac{M_{GC}}{M_{tot}(r_c)}\right]^{\frac{1}{3}} \left(\frac{r_c}{r_p}\right)^{\frac{1}{2}} \ , \tag{3.2}$$

where r_p is the pericentric radius of the stream orbit. We calibrate the dimensionless coefficient k_z on our numerical results, finding $k_z = 0.45$. This simple model well reproduces the undisturbed, constant vertical angular width of streams with different properties. As mentioned earlier, we also use the comparison in Fig. 4 to calibrate the magnitude of the Coulomb logarithm, which we fix at $\ln\Lambda = 9.6$. As shown by the same panel, we find that a constant Coulomb logarithm well describes the evolution of our disturbed streams[3]. Shaded areas closely follow the predicted dependence with time, highlighting how a diffusive description of the heating process is appropriate for the evolution of the vertical thickness.

The right panel of Figure 5 pertains to the thickness of the stream in the orbital plane. We measure the mean angular width in the plane of the stream as the standard deviation of the distribution of angular distances from the centerline of the stream (defined by a spline interpolation), over all particles that are no longer bound to the progenitor GC. Similarly to the left panel, numerical results are displayed in terms of the combination $\left(\frac{\omega_\parallel^2-\omega_{\parallel,0}^2}{d\omega_\parallel^2/dt}\right)^{\frac{1}{2}}$ and we use the same Coulomb logarithm. Furthermore, we take $\omega_{\parallel,0} = \omega_{z,0}$, as defined in Eqn. (3.2), and ignore that the unperturbed angular width in the orbital plane evolves linearly with time. This causes a departure between the predicted width

$$\left(\frac{\omega_\parallel^2-\omega_{\parallel,0}^2}{d\omega_\parallel^2/dt}\right)^{\frac{1}{2}} = t^{\frac{3}{2}} \ , \tag{3.3}$$

and what observed in the numerical experiments: shaded areas lie systematically above our model prediction, especially for the case of eccentric streams, which have a comparatively faster unperturbed growth rate. We are however not worried by this as this simplification makes our analytic model inherently conservative.

[3]We would expect the Coulomb logarithm to grow in magnitude as streams become thicker with time, but our simulations do not suggest that this adjustment is needed in the regime we are exploring here.

Table 1. Properties adopted for the cosidered Milky Way streams.

Stream	pericenter [kpc]	apocenter [kpc]	prog. mass $\log M_{GC}/M_\odot$	sky-projected width	Refs.
Palomar 5	7 ± 1	19 ± 0.5	4	FWHM= 120 pc	[48, 55, 56]
GD1	13 ± 1	22 ± 2	4	$\sigma = 12'$	[34, 48, 60]
Ophiucus	3.6 ± 0.1	16.8 ± 0.5	3.4	$\sigma = 4'$	[58, 61]
Acheron	3.5 ± 0.8	9.2 ± 3.3	4	FWHM= 60 pc	[57]
Cocytos	4.9 ± 0.2	12.5 ± 0.2	4	FWHM= 140 pc	[57]
Lethe	7.7 ± 0.4	17.3 ± 0.5	4	FWHM= 95 pc	[57]

4 First constraints on the axion mass

We use our analytical model to provide a first early constraint on the axion mass. In the presence of dark matter subhaloes or of additional baryonic perturbations streams will thicken beyond our model predictions. Therefore, our model quantifies the minimum width of streams in FDM haloes, which can be used to establish a lower limit for the axion mass m_{22}.

We use pre-Gaia literature data for six Milky Way streams: Palomar 5 [33], Ophiucus [58], GD1 [34], Acheron, Cocytos and Lethe [57], and we collect adopted values in Table 1. For each stream, we compare the observed angular width with what predicted by our model as a function of the axion mass, and we interpret this comparison as a bound on m_{22} using the following model likelihood:

$$\mathcal{L}(m_{22}) = \begin{cases} \exp\left[-\frac{1}{2}\left(\left(\omega_{obs} - \omega_{mod}\right)/\Delta\omega\right)^2\right] & \text{if } \omega_{obs} < \omega_{mod} \\ 1 & \text{otherwise,} \end{cases} . \tag{4.1}$$

The model angular thickness ω_{mod} depends on a number of nuisance astrophysical parameters. First, we require a model for the Galactic potential. As suggested by the approximately constant rotation curve of the Galaxy in the region of interest [62, 63], we adopt a logarithmic total gravitational potential, and take that the time-averaged dark matter density distribution follows a NFW density profile. We assume uncorrelated normally-distributed probability distributions for the following nuisance parameters and marginalise over them: *(i)* total circular velocity and solar radius, respectively $v_c = 220 \pm 10$ km s^{-1} and $R_\odot = 8.25 \pm 0.2$ kpc [62, 64]; *(ii)* local dark matter density and concentration of the dark halo, respectively $\rho_\odot = 10^{7\pm0.11} M_\odot$ kpc^{-3} and $c = 10 \pm 1$ [49, 65, 66].

Second, we require orbital properties for the different streams as well as structural properties for their progenitors. Pericentric and apocentric radii of the different streams are relatively well measured: we use these together with the mass model above to produce probability distributions for the circularity j and circular radius r_c for each stream. Obtaining estimates of the progenitor GC mass and age is more challenging. We remain conservative on both these quantities: (i) we adopt the progenitor masses listed in Table 1 and (ii) we estimate stream ages based on the lengths of the observed (section of) each stream. We get respectively 3, 5, 1.5, 5, 6, 1.5 Gyr for Palomar 5, GD1, Acheron, Cocytos and Lethe and Ophiucus, in line with other estimates in the literature [48, 55]. Finally, in addition to marginalizing over the astrophysical parameters listed so far, we also account for any additional uncertainty – in either the observed width and/or our model prediction – using a standard deviation of $\Delta\omega = 0.15 \times \omega_{obs}$ when computing the likelihood (4.1).

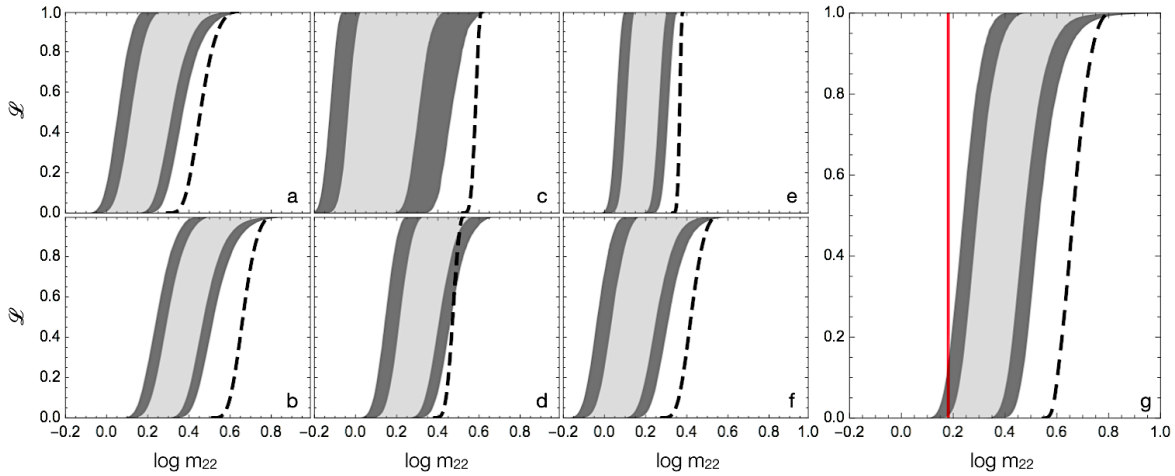

Figure 5. Constraints on the axion mass m_{22} from the width of individual Milky Way streams (respectively Palomar 5, Ophiucus, Acheron, Cocytos, Lethe and GD1 in panels *a* to *f*). Panel *g* displays the joint constraint, corresponding to a lower limit of $\log m_{22} > 0.18$, as shown by the red vertical line.

Use of an individual set of values for the astrophysical parameters and Eqn. (4.1) provides a profile for the likelihood $\mathcal{L}(m_{22})$ for each of our six streams, and therefore an exclusion region for the axion mass. By sampling the probability distributions of all nuisance parameters, we construct the shaded areas in the panels *a* to *f* in Figure 5. Each panel displays the 1-σ and 2-σ regions for the profiles of the likelihood $\mathcal{L}$, as a function of the axion mass m_{22}. From *a* to *f*, the different panels show our inference for Palomar 5, Ophiucus, Acheron, Lethe, Cocytos and GD1, respectively. Panel *g* shows the combined inference, assuming uncorrelated measurements. As we cannot attribute the thickness of the observed streams to FDM turbulence alone, the upper bounds of the shaded areas in Fig. 5 cannot be interpreted as upper bounds for the axion mass. However, as any additional form of heating would be simply added to the one caused by FDM, Fig. 5 provides valid lower bounds.

To derive nominal lower bounds for the axion mass we take the full sample of joint likelihood profiles $\mathcal{L}(m_{22})$ in panel *g* and, at any fixed m_{22} consider the top 95% quantile. This defines an exclusion region that is valid for 95% of all sets of nuisance parameters. For this choice, a 2-σ lower limit corresponds to $\log m_{22} > 0.18$, as shown in panel *g* by a vertical red line. Use of the likelihood profile $\mathcal{L}(m_{22})$ corresponding to the top 84% quantile over all sets of nuisance parameters together with a 1-σ exclusion would give us a tighter limit of $\log m_{22} > 0.3$.

Reduced uncertainties on the properties of the considered streams as well as on the other astrophysical parameters will allow for tighter constraints in the future. For instance, the total length of several of the used streams is currently unknown, as they appear truncated by the sky coverage of the survey in which they have been first discovered [57, 60]. The dashed lines in Figure 2 show profiles for the likelihood (9) that result from less conservative assumptions on the ages of our streams (respectively 4, 9, 4, 8, 9, 4 Gyr for Palomar 5, GD1, Acheron, Cocytos, Lethe and Ophiucus). These likelihood profiles adopt the fiducial values for the reported astrophysical parameters and an uncertainty of 3% for the observed average thickness of each stream, $\Delta\omega$. As shown in panel *g*, this would correspond to a joint 2-σ lower limit of $\log m_{22} > 0.6$. Parallel use of kinematic data would also strengthen results.

5 Discussion and Conclusions: an independent dynamical probe of FDM

We have shown that the turbulent behavior of FDM haloes produces observable dynamical heating of the kinematically cold stellar streams of GCs. Using a phenomenological description of the fluctuating dark matter density field, we have shown that this effect can be important for thin stellar streams in the Milky Way and that it is potentially observable for the range of axion masses that is interesting for cosmology. This shows the promise for obtaining independent local dynamical constraints to FDM.

Currently available constraints to the axion mass are all similarly derived from modelling the power spectrum of the Lyman-α forest [67–69]. These studies consistently appear to disfavour the range of axion masses that would result in significant astrophysical implications. Taken at face value, these studies rule out FDM models with $m_{22} \lesssim 20$, entirely excluding the window of boson masses required to alleviate the small-scale tensions with the CMD model. Since these results all rely on the same physics and on similar modelling, it is important to identify different, independent probes of the axion mass. It has been claimed, in fact, that a number of astrophysical effects may cause the constraints above to be substantially relaxed, perhaps by an order of magnitude [18]. Based on entirely different physics, the perturbation and heating of GC streams in the Milky Way can provide us with such a fully independent test of the FDM model.

For this purpose, we have constructed an analytic model for the effects of quantum turbulence on the stream thickness. This is based on a quasiparticle effective model of the turbulent density field of FDM haloes. We find that streams experience a process of diffusive heating, causing their internal velocity dispersion and vertical angular width to grow as $t^{1/2}$. Because of the secular dynamics of the stream, the evolution of the angular width in the orbital plane is faster. We have tested these scalings using a suite of tailored numerical simulations and found that our analytic model well reproduces the process of diffusive dynamical heating caused by the random encounters with the FDM clumps.

Using conservative assumptions on the properties of six Milky Way streams and pre-Gaia literature data, we have derived a first lower limit of $m_a > 1.5 \times 10^{-22}$ eV. Improved data for the same streams and tighter constraints on the gravitational potential of the Galaxy will likely allow for a correspondingly tighter limit. Furthermore, the detection of previously unknown GC streams in the central regions of the Galaxy may also allow new stringent limits. Figure 6 shows the minimum angular width (in degrees) predicted by Eqs. (2.7) and (2.14) for young streams (age $t = 2$ Gyr) with progenitors of mass $\log(M_{GC}/M_\odot) = 4$ and almost circular orbits ($j = 0.85$), for a range of orbital energies and axion masses. The detection of any single stream that is thinner than predicted here would essentially rule out a significant range of the parameter space.

In this paper, we have focussed on the readily observable mean angular width and velocity dispersion of streams. However, future observations of the detailed properties of the stream's density and kinematic fields will provide additional constraining power, as the heating process by the quantum fluctuations is not fully diffusive, as shown by Figures 2 and 3. In fact, the perturbations caused by FDM turbulence and by low-mass CDM subhaloes may be degenerate in some regimes, especially within analyses that concentrate on a single stream. Analyses based on a set of streams with different orbital energies will be able to disentangle the two effects, based on the markedly different dependence on galactocentric distance of the heating caused by FDM turbulence.

Though guided by the results of current self-consistent FDM simulations, the current

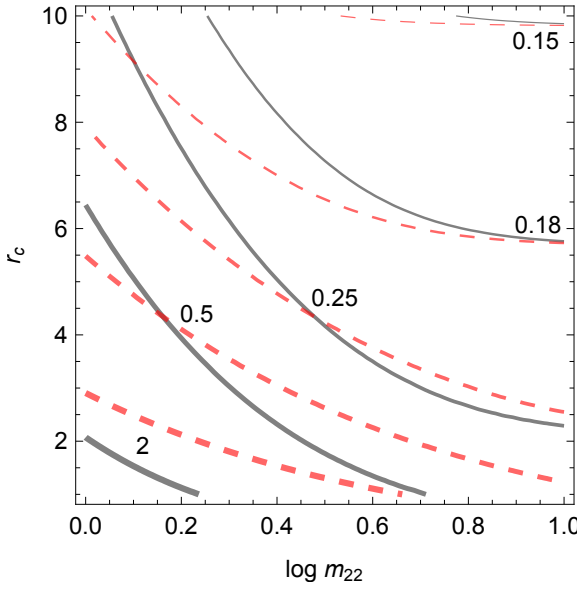

Figure 6. The minimum angular width in degrees for young streams (age $t = 2$ Gyr) with progenitors of mass $\log(M_{GC}/M_\odot) = 4$ and orbital circularity $j = 0.85$. The widths in the direction perpendicular and parallel to the orbital plane are displayed by black full lines and red dashed lines.

model remains however quite simplified. Future self-consistent simulations of FDM haloes will be able to better resolve the dynamics of individual oscillations in the dark matter density field. The analytic framework we have presented can easily be improved to incorporate a more faithful description of the properties of real quantum clumps. For instance, a better statistical description of the spectrum of effective masses and of their motion would be beneficial, together with a characterization of any secondary dependences between the two quantities. We anticipate that the analytic model presented here can be used in combination with future numerical results from self-consistent simulations to more accurately predict the effect of dynamical heating. Thanks to the Gaia mission and upcoming Galactic surveys [70–74], dynamical heating of stellar streams in the inner Milky Way provides a promising novel method for setting independent constraints on FDM models, with the potential for improved and competitive limits.

Acknowledgments

This work was supported in part by the Black Hole Initiative, which is funded by a JTF grant.

References

[1] R. D. Peccei and H. R. Quinn. CP conservation in the presence of pseudoparticles. *Physical Review Letters*, 38:1440–1443, June 1977.

[2] F. Wilczek. Problem of strong P and T invariance in the presence of instantons. *Physical Review Letters*, 40:279–282, January 1978.

[3] S. Weinberg. A new light boson? *Physical Review Letters*, 40:223–226, January 1978.

[4] D. N. Spergel and P. J. Steinhardt. Observational Evidence for Self-Interacting Cold Dark Matter. *Physical Review Letters*, 84:3760–3763, April 2000.

[5] W. Hu, R. Barkana, and A. Gruzinov. Fuzzy Cold Dark Matter: The Wave Properties of Ultralight Particles. *Physical Review Letters*, 85:1158–1161, August 2000.

[6] T. Matos, F. S. Guzmán, and L. A. Ureña-López. Scalar field as dark matter in the universe. *Classical and Quantum Gravity*, 17:1707–1712, April 2000.

[7] P. J. E. Peebles. Fluid Dark Matter. *ApJL*, 534:L127–L129, May 2000.

[8] J. Goodman. Repulsive dark matter. *New Astronomy*, 5:103–107, April 2000.

[9] B. Li, T. Rindler-Daller, and P. R. Shapiro. Cosmological constraints on Bose-Einstein-condensed scalar field dark matter. *Physical Review D*, 89(8):083536, April 2014.

[10] R. Hlozek, D. Grin, D. J. E. Marsh, and P. G. Ferreira. A search for ultralight axions using precision cosmological data. *Physical Review D*, 91(10):103512, May 2015.

[11] R. Hložek, D. J. E. Marsh, and D. Grin. Using the full power of the cosmic microwave background to probe axion dark matter. *MNRAS*, 476:3063–3085, May 2018.

[12] J. A. Frieman, C. T. Hill, A. Stebbins, and I. Waga. Cosmology with Ultralight Pseudo Nambu-Goldstone Bosons. *Physical Review Letters*, 75:2077–2080, September 1995.

[13] L. Amendola and R. Barbieri. Dark matter from an ultra-light pseudo-Goldsone-boson. *Physics Letters B*, 642:192–196, November 2006.

[14] D. J. E. Marsh and P. G. Ferreira. Ultralight scalar fields and the growth of structure in the Universe. *Physical Review D*, 82(10):103528, November 2010.

[15] J.-W. Lee and I.-G. Koh. Galactic halos as boson stars. *Physical Review D*, 53:2236–2239, February 1996.

[16] F. S. Guzmán, T. Matos, and H. B. Villegas. Scalar fields as dark matter in spiral galaxies: comparison with experiments. *Astronomische Nachrichten*, 320:97, 1999.

[17] D. J. E. Marsh. Axion cosmology. *Physics Reports*, 643:1–79, July 2016.

[18] L. Hui, J. P. Ostriker, S. Tremaine, and E. Witten. Ultralight scalars as cosmological dark matter. *Physical Review D*, 95(4):043541, February 2017.

[19] D. J. E. Marsh and A.-R. Pop. Axion dark matter, solitons and the cusp-core problem. *MNRAS*, 451:2479–2492, August 2015.

[20] S.-R. Chen, H.-Y. Schive, and T. Chiueh. Jeans analysis for dwarf spheroidal galaxies in wave dark matter. *MNRAS*, 468:1338–1348, June 2017.

[21] A. X. González-Morales, D. J. E. Marsh, J. Peñarrubia, and L. A. Ureña-López. Unbiased constraints on ultralight axion mass from dwarf spheroidal galaxies. *MNRAS*, 472:1346–1360, December 2017.

[22] D. H. Weinberg, J. S. Bullock, F. Governato, R. Kuzio de Naray, and A. H. G. Peter. Cold dark matter: Controversies on small scales. *Proceedings of the National Academy of Science*, 112:12249–12255, October 2015.

[23] J. S. Bullock and M. Boylan-Kolchin. Small-Scale Challenges to the ΛCDM Paradigm. *ARAA*, 55:343–387, August 2017.

[24] M. Gleiser. Stability of boson stars. *Physical Review D*, 38:2376–2385, October 1988.

[25] S.-J. Sin. Late-time phase transition and the galactic halo as a Bose liquid. *Physical Review D*, 50:3650–3654, September 1994.

[26] P.-H. Chavanis. Mass-radius relation of Newtonian self-gravitating Bose-Einstein condensates with short-range interactions. I. Analytical results. *Physical Review D*, 84(4):043531, August 2011.

[27] H.-Y. Schive, M.-H. Liao, T.-P. Woo, S.-K. Wong, T. Chiueh, T. Broadhurst, and W.-Y. P. Hwang. Understanding the Core-Halo Relation of Quantum Wave Dark Matter from 3D Simulations. *Physical Review Letters*, 113(26):261302, December 2014.

[28] P. Mocz, M. Vogelsberger, V. H. Robles, J. Zavala, M. Boylan-Kolchin, A. Fialkov, and L. Hernquist. Galaxy formation with BECDM - I. Turbulence and relaxation of idealized haloes. *MNRAS*, 471:4559–4570, November 2017.

[29] J. F. Navarro, C. S. Frenk, and S. D. M. White. The Structure of Cold Dark Matter Halos. *ApJ*, 462:563, May 1996.

[30] P. Mocz, L. Lancaster, A. Fialkov, F. Becerra, and P.-H. Chavanis. On the Schrodinger-Poisson–Vlasov-Poisson correspondence. *ArXiv e-prints*, January 2018.

[31] M. Kobayashi and M. Tsubota. Kolmogorov Spectrum of Quantum Turbulence. *Journal of the Physical Society of Japan*, 74:3248–3258, December 2005.

[32] A. W. Baggaley, J. Laurie, and C. F. Barenghi. Vortex-Density Fluctuations, Energy Spectra, and Vortical Regions in Superfluid Turbulence. *Physical Review Letters*, 109(20):205304, November 2012.

[33] M. Odenkirchen, E. K. Grebel, A. Kayser, H.-W. Rix, and W. Dehnen. Kinematics of the Tidal Debris of the Globular Cluster Palomar 5. *AJ*, 137:3378–3387, February 2009.

[34] S. E. Koposov, H.-W. Rix, and D. W. Hogg. Constraining the Milky Way Potential with a Six-Dimensional Phase-Space Map of the GD-1 Stellar Stream. *ApJ*, 712:260–273, March 2010.

[35] R. A. Ibata, G. F. Lewis, M. J. Irwin, and T. Quinn. Uncovering cold dark matter halo substructure with tidal streams. *MNRAS*, 332:915–920, June 2002.

[36] K. V. Johnston, D. N. Spergel, and C. Haydn. How Lumpy Is the Milky Way's Dark Matter Halo? *ApJ*, 570:656–664, May 2002.

[37] R. G. Carlberg. Dark Matter Sub-halo Counts via Star Stream Crossings. *ApJ*, 748:20, March 2012.

[38] D. Erkal, S. E. Koposov, and V. Belokurov. A sharper view of Pal 5's tails: discovery of stream perturbations with a novel non-parametric technique. *MNRAS*, 470:60–84, September 2017.

[39] J. Bovy, D. Erkal, and J. L. Sanders. Linear perturbation theory for tidal streams and the small-scale CDM power spectrum. *MNRAS*, 466:628–668, April 2017.

[40] N. Banik, G. Bertone, J. Bovy, and N. Bozorgnia. Probing the nature of dark matter particles with stellar streams. *ArXiv e-prints*, April 2018.

[41] N. C. Amorisco, F. A. Gómez, S. Vegetti, and S. D. M. White. Gaps in globular cluster streams: giant molecular clouds can cause them too. *MNRAS*, 463:L17–L21, November 2016.

[42] K. Hattori, D. Erkal, and J. L. Sanders. Shepherding tidal debris with the Galactic bar: the Ophiuchus stream. *MNRAS*, 460:497–512, July 2016.

[43] S. Pearson, A. M. Price-Whelan, and K. V. Johnston. Gaps and length asymmetry in the stellar stream Palomar 5 as effects of Galactic bar rotation. *Nature Astronomy*, 1:633–639, September 2017.

[44] V. Springel, J. Wang, M. Vogelsberger, A. Ludlow, A. Jenkins, A. Helmi, J. F. Navarro, C. S. Frenk, and S. D. M. White. The Aquarius Project: the subhaloes of galactic haloes. *MNRAS*, 391:1685–1711, December 2008.

[45] S. Garrison-Kimmel, A. Wetzel, J. S. Bullock, P. F. Hopkins, M. Boylan-Kolchin, C.-A. Faucher-Giguère, D. Kereš, E. Quataert, R. E. Sanderson, A. S. Graus, and T. Kelley. Not so

lumpy after all: modelling the depletion of dark matter subhaloes by Milky Way-like galaxies. *MNRAS*, 471:1709–1727, October 2017.

[46] T. Sawala, P. Pihajoki, P. H. Johansson, C. S. Frenk, J. F. Navarro, K. A. Oman, and S. D. M. White. Shaken and stirred: the Milky Way's dark substructures. *MNRAS*, 467:4383–4400, June 2017.

[47] J. Diemand, M. Kuhlen, P. Madau, M. Zemp, B. Moore, D. Potter, and J. Stadel. Clumps and streams in the local dark matter distribution. *Nat*, 454:735–738, August 2008.

[48] D. Erkal, V. Belokurov, J. Bovy, and J. L. Sanders. The number and size of subhalo-induced gaps in stellar streams. *MNRAS*, 463:102–119, November 2016.

[49] J. I. Read. The local dark matter density. *Journal of Physics G Nuclear Physics*, 41(6):063101, June 2014.

[50] A. Helmi and S. D. M. White. Building up the stellar halo of the Galaxy. *MNRAS*, 307:495–517, August 1999.

[51] D. Erkal, J. L. Sanders, and V. Belokurov. Stray, swing and scatter: angular momentum evolution of orbits and streams in aspherical potentials. *MNRAS*, 461:1590–1604, September 2016.

[52] K. V. Johnston, P. D. Sackett, and J. S. Bullock. Interpreting Debris from Satellite Disruption in External Galaxies. *ApJ*, 557:137–149, August 2001.

[53] N. C. Amorisco. On feathers, bifurcations and shells: the dynamics of tidal streams across the mass scale. *MNRAS*, 450:575–591, June 2015.

[54] F. Renaud, M. Gieles, and C. M. Boily. Evolution of star clusters in arbitrary tidal fields. *MNRAS*, 418:759–769, December 2011.

[55] A. H. W. Küpper, E. Balbinot, A. Bonaca, K. V. Johnston, D. W. Hogg, P. Kroupa, and B. X. Santiago. Globular Cluster Streams as Galactic High-Precision Scales – the Poster Child Palomar 5. *ApJ*, 803:80, April 2015.

[56] M. Odenkirchen, E. K. Grebel, W. Dehnen, H.-W. Rix, B. Yanny, H. J. Newberg, C. M. Rockosi, D. Martínez-Delgado, J. Brinkmann, and J. R. Pier. The Extended Tails of Palomar 5: A 10deg Arc of Globular Cluster Tidal Debris. *AJ*, 126:2385–2407, November 2003.

[57] C. J. Grillmair. Four New Stellar Debris Streams in the Galactic Halo. *ApJ*, 693:1118–1127, March 2009.

[58] B. Sesar, J. Bovy, E. J. Bernard, N. Caldwell, J. G. Cohen, M. Fouesneau, C. I. Johnson, M. Ness, A. M. N. Ferguson, N. F. Martin, A. M. Price-Whelan, H.-W. Rix, E. F. Schlafly, W. S. Burgett, K. C. Chambers, H. Flewelling, K. W. Hodapp, N. Kaiser, E. A. Magnier, I. Platais, J. L. Tonry, C. Waters, and R. F. G. Wyse. The Nature and Orbit of the Ophiuchus Stream. *ApJ*, 809:59, August 2015.

[59] V. Springel. The cosmological simulation code GADGET-2. *MNRAS*, 364:1105–1134, December 2005.

[60] C. J. Grillmair and O. Dionatos. Detection of a 63deg Cold Stellar Stream in the Sloan Digital Sky Survey. *ApJL*, 643:L17–L20, May 2006.

[61] E. J. Bernard, A. M. N. Ferguson, E. F. Schlafly, M. Abbas, E. F. Bell, N. R. Deacon, N. F. Martin, H.-W. Rix, B. Sesar, C. T. Slater, J. Peñarrubia, R. F. G. Wyse, W. S. Burgett, K. C. Chambers, P. W. Draper, K. W. Hodapp, N. Kaiser, R.-P. Kudritzki, E. A. Magnier, N. Metcalfe, J. S. Morgan, P. A. Price, J. L. Tonry, R. J. Wainscoat, and C. Waters. Serendipitous discovery of a thin stellar stream near the Galactic bulge in the Pan-STARRS1 3π Survey. *MNRAS*, 443:L84–L88, September 2014.

[62] J. Bland-Hawthorn and O. Gerhard. The Galaxy in Context: Structural, Kinematic, and Integrated Properties. *ARAA*, 54:529–596, September 2016.

[63] K. Sysoliatina, A. Just, O. Golubov, Q. A. Parker, E. K. Grebel, G. Kordopatis, T. Zwitter, J. Bland-Hawthorn, B. K. Gibson, A. Kunder, U. Munari, J. Navarro, W. Reid, G. Seabroke, M. Steinmetz, and F. Watson. The local rotation curve of the Milky Way based on SEGUE and RAVE data. *ArXiv e-prints*, February 2018.

[64] J. Bovy, A. Bahmanyar, T. K. Fritz, and N. Kallivayalil. The Shape of the Inner Milky Way Halo from Observations of the Pal 5 and GD–1 Stellar Streams. *ApJ*, 833:31, December 2016.

[65] A. V. Macciò, A. A. Dutton, and F. C. van den Bosch. Concentration, spin and shape of dark matter haloes as a function of the cosmological model: WMAP1, WMAP3 and WMAP5 results. *MNRAS*, 391:1940–1954, December 2008.

[66] A. D. Ludlow, S. Bose, R. E. Angulo, L. Wang, W. A. Hellwing, J. F. Navarro, S. Cole, and C. S. Frenk. The mass-concentration-redshift relation of cold and warm dark matter haloes. *MNRAS*, 460:1214–1232, August 2016.

[67] V. Iršič, M. Viel, M. G. Haehnelt, J. S. Bolton, and G. D. Becker. First Constraints on Fuzzy Dark Matter from Lyman-α Forest Data and Hydrodynamical Simulations. *Physical Review Letters*, 119(3):031302, July 2017.

[68] E. Armengaud, N. Palanque-Delabrouille, C. Yèche, D. J. E. Marsh, and J. Baur. Constraining the mass of light bosonic dark matter using SDSS Lyman-α forest. *MNRAS*, 471:4606–4614, November 2017.

[69] T. Kobayashi, R. Murgia, A. De Simone, V. Iršič, and M. Viel. Lyman-α constraints on ultralight scalar dark matter: Implications for the early and late universe. *Physical Review D*, 96(12):123514, December 2017.

[70] Gaia Collaboration, A. G. A. Brown, A. Vallenari, T. Prusti, J. H. J. de Bruijne, C. Babusiaux, and C. A. L. Bailer-Jones. Gaia Data Release 2. Summary of the contents and survey properties. *ArXiv e-prints*, April 2018.

[71] DESI Collaboration, A. Aghamousa, J. Aguilar, S. Ahlen, S. Alam, L. E. Allen, C. Allende Prieto, J. Annis, S. Bailey, C. Balland, and et al. The DESI Experiment Part I: Science,Targeting, and Survey Design. *ArXiv e-prints*, October 2016.

[72] LSST Science Collaboration, P. A. Abell, J. Allison, S. F. Anderson, J. R. Andrew, J. R. P. Angel, L. Armus, D. Arnett, S. J. Asztalos, T. S. Axelrod, and et al. LSST Science Book, Version 2.0. *ArXiv e-prints*, December 2009.

[73] R. S. de Jong, S. C. Barden, O. Bellido-Tirado, J. G. Brynnel, S. Frey, D. Giannone, R. Haynes, D. Johl, D. Phillips, O. Schnurr, J. C. Walcher, R. Winkler, W. R. Ansorge, S. Feltzing, R. G. McMahon, G. Baker, P. Caillier, T. Dwelly, W. Gaessler, O. Iwert, H. G. Mandel, N. A. Piskunov, J. H. Pragt, N. A. Walton, T. Bensby, M. Bergemann, C. Chiappini, N. Christlieb, M.-R. L. Cioni, S. Driver, A. Finoguenov, A. Helmi, M. J. Irwin, F.-S. Kitaura, J.-P. Kneib, J. Liske, A. Merloni, I. Minchev, J. Richard, and E. Starkenburg. 4MOST: the 4-metre Multi-Object Spectroscopic Telescope project at preliminary design review. In *Ground-based and Airborne Instrumentation for Astronomy VI*, volume 9908 of *Proc. of the SPIE*, page 99081O, August 2016.

[74] G. Dalton, S. Trager, D. C. Abrams, P. Bonifacio, J. A. L. Aguerri, K. Middleton, C. Benn, K. Dee, F. Sayède, I. Lewis, J. Pragt, S. Pico, N. Walton, J. Rey, C. Allende Prieto, J. Peñate, E. Lhome, T. Agócs, J. Alonso, D. Terrett, M. Brock, J. Gilbert, E. Schallig, A. Ridings, I. Guinouard, M. Verheijen, I. Tosh, K. Rogers, M. Lee, I. Steele, R. Stuik, N. Tromp, A. Jaskó, E. Carrasco, S. Farcas, J. Kragt, D. Lesman, G. Kroes, C. Mottram, S. Bates, L. F. Rodriguez, F. Gribbin, J. M. Delgado, J. M. Herreros, C. Martin, D. Cano, R. Navarro, M. Irwin, J. Lewis, E. Gonzalez Solares, D. Murphy, C. Worley, R. Bassom, N. O'Mahoney,

A. Bianco, C. Zurita, R. ter Horst, E. Molinari, M. Lodi, J. Guerra, A. Martin, A. Vallenari, B. Salasnich, A. Baruffolo, S. Jin, V. Hill, D. Smith, J. Drew, B. Poggianti, M. Pieri, L. Dominquez Palmero, and C. Farina. Final design and progress of WEAVE: the next generation wide-field spectroscopy facility for the William Herschel Telescope. In *Ground-based and Airborne Instrumentation for Astronomy VI*, volume 9908 of *Proc. of the SPIE*, page 99081G, August 2016.